

Polymorphism in the Packing of Aquaporin-1 Tetramers in 2-D Crystals

Gang Ren, Anchi Cheng, Peter Melnyk, and Alok K. Mitra¹

Department of Cell Biology, The Scripps Research Institute, 10550 North Torrey Pines Road, La Jolla, California 92037

Received October 14, 1999, and in revised form December 6, 1999

Hitherto, the packing arrangement of the aquaporin-1 (AQP1) tetramer in 2-dimensional (2-D) crystals (two-sided plane group $p4_21_2$) was observed to be largely similar (canonical crystal form) despite the difference in the source of the protein, the glycosylation state of the protein, the type of lipids, and the ratio of lipid to protein in the crystallization mixture. We report here our observation that the packing of AQP1 tetramers shows polymorphism in 2-D crystals generated in dioleoyl phosphatidylcholine bilayers. Apart from the canonical form, three additional allomorphs were identified. One was observed when small (0.25) lipid to protein ratio was used in the crystallization mixture while the other two were observed when the divalent cation content in the canonical crystals was modified. The various allomorphs were distinguished by different relative orientations of the AQP1 tetramer viewed in projection. The same, two-sided plane group $p4_21_2$ and similar unit cell dimensions were maintained in the different allomorphs as established by analysis of images of frozen-hydrated, nominally untilted crystals. Our results indicate that the interaction between the AQP1 monomers at the interface of the tetramers is flexible and is also strongly influenced by Mg^{2+} ions with the cation effect materializing because of the intrinsic fluidity of the membrane. © 2000

Academic Press

Key Words: aquaporin; membrane-protein structure; 2-dimensional crystal; and electron crystallography.

INTRODUCTION

Aquaporins are intrinsic membrane proteins found in both eukaryotes and prokaryotes where they serve as channels for rapid dissipation of osmotic gradients across the lipid bilayer (Agre *et al.*, 1995; Verkman *et al.*, 1996). The abundantly expressed, partially glycosylated, AQP1 (earlier called CHIP28) channel is the archetype in the aquaporin family

whose members belong to the MIP (major intrinsic protein) superfamily (Gorin *et al.*, 1984). There is a general consensus that AQP1 selectively transports water (Zeidel *et al.*, 1994), although recent reports have implicated CO_2 permeability (Nakhoul *et al.*, 1998; Prasad *et al.*, 1998)).

2-D (2-dimensional) crystals of AQP1 have been used to examine the structure using electron crystallography which has proven to be invaluable for determining high-resolution 3-D structures of membrane proteins (Grigorieff *et al.*, 1996; Henderson *et al.*, 1990; Kimura *et al.*, 1997; Kühlbrandt *et al.*, 1994). Generation of 2-D crystals of AQP1 was reported by Walz *et al.* (1994) and later by Mitra *et al.* (1994). Projection maps of AQP1 were determined by electron cryo-crystallography by three groups (Jap and Li, 1995; Mitra *et al.*, 1995; Walz *et al.*, 1995) who used different conditions for 2-D crystallization and specimen preservation for microscopy. Walz *et al.* (1995) used glucose-embedded native, partially glycosylated AQP1 from human erythrocytes that were crystallized in lipids extracted from *Escherichia coli*. Glucose embedding was also employed by Jap and Li (1995) who used native, bovine AQP1 crystallized in dimyristoyl phosphatidylcholine (DMPC). We (Mitra *et al.*, 1995) crystallized deglycosylated, human erythrocyte AQP1 in dioleoyl phosphatidylcholine (DOPC) bilayers and examined the frozen-hydrated crystals preserved in vitrified buffer. Notwithstanding the differences stated above, the three projection maps revealed overall similarities characterized by tetrameric packing of the AQP1 monomers and multiple density peaks in each monomer suggestive of α -helices. The orientation and packing of the 6 α -helices were visualized in detail in the 3-D density maps calculated by the three groups (Li *et al.*, 1997; Walz *et al.*, 1997; Cheng *et al.*, 1997).

A feature of the three projection maps reported by the three groups was the similar orientation of the AQP1 tetramers in the unit cell. Based on this observation, it has been suggested (Hasler *et al.*, 1998) that a single and dominant set of specific protein-protein interactions exists between the AQP1 tetramers in the 2-D crystals in lipid bilayers. We

¹ To whom correspondence should be addressed. Fax: (858) 784-9927. E-mail: mitra@scripps.edu.

report here our observation that the packing of AQP1 tetramers in 2-D crystals generated in DOPC bilayers can show polymorphism. Variations in the packing arrangement were observed either when small lipid to protein ratio (LPR) was used or when the divalent cation content was modified by posttreatment of the crystals. This variability suggests that, between AQP1 tetramers, there is a flexibility in the direct protein-protein interaction and/or indirect protein-lipid interactions which leads to alterations in the packing scheme.

MATERIALS AND METHODS

2-D crystallization. Highly ordered 2-D crystals of deglycosylated AQP1 were prepared (Mitra *et al.*, 1995) by reconstitution of protein into DOPC bilayers. Outdated human erythrocytes (San Diego blood bank) were used to generate protein purified (van Hoek *et al.*, 1995) in the detergent *n*-octyl- β -D-glucopyranoside (OG; Anatrace, Maumee, OH). The concentrations of protein, lipid, and detergent in the "canonical" crystallization cocktail were 1.0 mg/ml, 0.33 mg/ml, and 70–120 mM respectively in 20 mM NaP_i, 100 mM NaCl, 0.1 mM EDTA, 0.025% NaN₃, pH 7.2 (buffer A). Protein reconstitution and crystallization were achieved after minimizing the amount of detergent in the protein-lipid-detergent mixture by dialyzing against 1000-fold excess buffer A for 8 days with change of buffer every 48 h. Hereafter, the canonical crystals are referred to as type I. The crystallization condition for the growth of type II crystals was the same as for type I except that the lipid concentration was 0.25 mg/ml. Further treatment of type I crystals was carried out as follows. One treatment consisted of removing EDTA in the suspension containing crystals by dialysis against 5000-fold excess buffer B (20 mM NaP_i, 100 mM NaCl, 0.025% NaN₃, pH 7.2) for 6 days. Another treatment was incorporation of Mg²⁺ ions into the crystalline suspension by first dialyzing the crystals against 5000-fold excess buffer B for 6 days followed by dialysis against 5000-fold excess buffer C (20 mM NaP_i, 100 mM NaCl, 2 mM MgCl₂, 0.025% NaN₃, pH 7.2) for 3 days and subsequent removal of unbound Mg²⁺ by dialysis against 5000-fold excess buffer B for 3 days. Degradation of protein in the crystals was checked by SDS-PAGE with a 12.5% polyacrylamide resolving gel and 4% stacking gel.

Preparation of frozen-hydrated ice-embedded specimens. Frozen-hydrated specimens were prepared in a cold room (4°C, ambient relative humidity 90%) using a plunge-freeze device (Dubochet *et al.*, 1988). Typically, reconstituted samples were allowed to settle for ~2 min on a 300-mesh molybdenum grid overlaid with a flat, continuous carbon film that had been rendered hydrophilic by glow-discharging (60–90 s) in a saturated atmosphere (0.05 to 0.10 Torr) of amylamine. The grid was blotted with a preheated filter paper for 10–30 s and then plunged into liquid ethane slush to achieve vitrification.

Data collection and processing. Minimal-dose, flood-beam images were collected using a Philips CM200FEG electron microscope operated at 200 kV at a nominal magnification of 50,000. Images were recorded on Kodak SO-163 films, which were developed for 11 min in full-strength Kodak D-19 developer under nitrogen burst. Images were assessed for their quality on an optical diffractometer and those displaying sharp spots, minimum drift, and astigmatism were chosen for processing. Selected areas of good images were digitized on a Perkin-Elmer PDS densitometer using an aperture and step size of 7 μ m. Image processing was carried out on a DEC/Alpha workstation following the protocol and the programs (MRC package) described in Henderson *et al.* (1990). The program ALLSPACE was used to ascertain the plane group symmetry. Images of a given crystal type were brought to the same origin based on the phases of all reflections with $IQ \leq 7$ (in the nomenclature of Henderson *et al.*, 1986).

Electron diffraction patterns from nominally untilted crystals of the canonical crystal form (type I) were digitized on a Perkin-Elmer PDS densitometer using an aperture and step size of 10 μ m and processed using a peak profile fitting algorithm (PICKPROF) in the MRC package (Baldwin and Henderson, 1984). A reflection was excluded if the average of the intensities of the Friedel pairs was less than their difference and greater than 5 times the standard deviation of such averages for all reflections in that pattern. The merging of the data from diffraction patterns involved scaling and application of isotropic temperature factor. The intensities of very-low-resolution (≥ 25 Å) spots in the diffraction pattern cannot be correctly estimated because of the extremely high background intensity caused by inelastic scattering. For such reflections, amplitudes derived from the images of the type I crystal were used after correcting for the CTF (using CTFAPPLY) and scaling by an appropriate scale factor based on strong

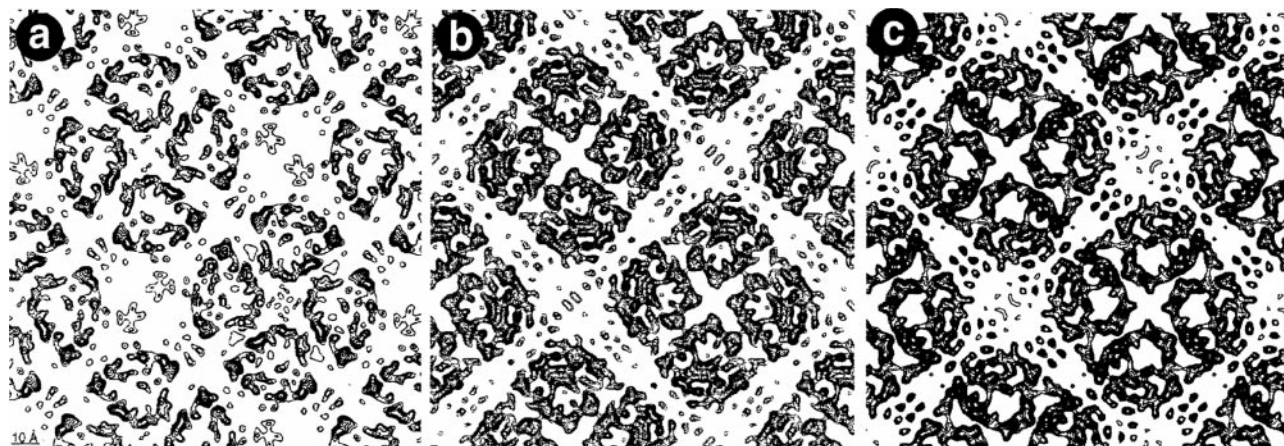


FIG. 1. Projection density map of AQP1 in type I crystal form that has been subjected to 3-D structural analysis. (a) Map at 3.5 Å resolution reproduced from Jap and Li (1995), (b) map at 3.5 Å resolution reproduced from Hasler *et al.* (1998), and (c) map at 3.7 Å resolution determined in the present study.

TABLE I
Phase Residual in Different Two-Sided Plane Groups for the Four Different Packing Allomorphs

Two-sided plane group	Type I (Image 1898)				Type II (Image 8464)				Type III (Image F291)				Type IV (Image I257)							
	Phase residual ^a and number of comparison		Phase residual ^b and number of comparison		Phase residual ^a and number of comparison		Phase residual ^b and number of comparison		Phase residual ^a and number of comparison		Phase residual ^b and number of comparison		Phase residual ^a and number of comparison		Phase residual ^b and number of comparison					
p1	22.4	522	16.3	522	24.6	488	17.9	488	24.4	410	17.8	410	21.0	568	15.2	568				
p2	33.7‡	261	16.9	522	32.5	36.1*	244	18.0	488	35.8	42.6†	205	21.3	410	35.5	20.3*	284	10.2	568	30.4
p12_b	82.2	214	53.4	16	22.8	79.9	193	48.2	14	25.0	77.3	154	24.0	12	24.8	84.0	245	44.9	14	21.3
p12_a	84.2	216	50.8	20	22.9	84.6	195	49.6	18	25.1	82.9	159	46.6	22	25.1	81.3	245	48.5	14	21.3
p12_b	23.0*	214	10.6	16	22.8	27.6‡	193	18.3	14	25.0	27.3‡	154	22.0	12	24.8	18.9*	245	6.8	14	21.3
p12_a	16.1*	216	15.4	20	22.9	18.7*	195	20.1	18	25.1	19.6*	159	21.1	22	25.1	17.6*	245	16.2	14	21.3
c12_b	82.2	214	53.4	16	22.8	79.9	193	48.2	14	25.0	77.3	154	24.0	12	24.8	84.0	245	44.9	14	21.3
c12_a	84.2	216	50.8	20	22.9	84.6	195	49.6	18	25.1	82.9	159	46.6	22	25.1	81.3	245	48.5	14	21.3
p222	67.3	691	16.9	522	26.2	68.2	632	18.1	488	28.9	67.2	518	21.3	410	28.8	61.8	774	10.2	568	24.4
p222b	61.7	691	41.3	522	26.2	62.7	632	40.9	488	28.9	60.8	518	40.1	410	28.8	63.0	774	42.1	568	24.4
p222a	65.2	691	41.6	522	26.2	67.8	632	42.8	488	28.9	66.2	518	41.0	410	28.8	62.1	774	41.4	568	24.4
p2212	24.9*	691	16.9	522	26.2	28.2*	632	18.1	488	28.9	31.0‡	518	21.3	410	28.8	19.0*	774	10.2	568	24.4
c222	67.3	691	16.9	522	26.2	68.2	632	18.1	488	28.9	67.2	518	21.3	410	28.8	61.8	774	10.2	568	24.4
p4	26.4*	713	16.9	522	26.1	26.6*	648	18.1	488	28.8	31.9‡	521	21.3	410	28.7	18.2*	764	10.2	568	24.5
p422	60.3	1576	16.9	522	24.1	60.5	1425	18.2	488	26.5	60.3	1116	21.3	410	26.4	57.3	1726	10.2	568	22.5
p4212	23.5*	1576	16.9	522	24.1	24.9*	1425	18.1	488	26.5	27.2*	1116	21.3	410	26.4	18.2*	1726	10.2	568	22.5

^a Versus other spots (90° random)—data included to 6.5 Å resolution.

^b Versus theoretical (45° random)—data included to 6.5 Å resolution.

^c Based on statistics taking Friedel weight into account.

* Acceptable suggestion based on the statistics; † possible suggestion based on the statistics; ‡ two-sided plane group, which also should be considered, based on the statistics.

reflections in the neighboring higher resolution shell (25–18 Å, e.g., the 5.1 reflection at 19.6 Å resolution).

All analyses of crystals other than the canonical type I crystals were based on images recorded from nominally untilted specimens. Except for type I crystals, projection maps were calculated by using phases and amplitudes from images boosted by a B-factor (–100) to compensate for resolution-dependent fall-off in image contrast (Schertler *et al.*, 1993). In the case of type I crystals, amplitudes were those obtained directly from nominally untilted electron diffraction patterns.

RESULTS AND DISCUSSION

Hitherto, in 2-D crystals the packing of AQP1 tetramers has been shown to be essentially similar (Fig. 1; Hasler *et al.*, 1998). Such crystals belong to what we call a type I form. The optical transforms of images recorded from crystals generated with lower LPR or from crystals in which the divalent-cation content was varied indicated different motifs for the distribution of strong, medium resolution (~16–10 Å) reflections when compared to that for the canonical (type I) crystal recorded at a similar level of defocus. In addition, the 4-fold symmetry was maintained as before. Based on the characteristic optical transforms, three additional allomorphs (type II, type III, and type IV) were identified. The type II form was seen when the lipid to protein ratio (weight/weight) in the crystallization cocktail was 1/3.5 or lower. This form was seen occasionally also at higher lipid to protein ratios, but was the abundant form at lower ratios. The other two allomorphs appeared upon alteration of divalent-cation content in the suspension containing type I crystals. Type III crystals

resulted upon removal of EDTA whereas type IV crystals were generated by exogenous addition of Mg²⁺. As in the case of type I crystals, results from ALLSPACE indicated the best agreement when the phases for each new allomorph were constrained by the symmetry of two-sided plane group p42₁2 (Table I). The dissimilarity between each new allomorph and the canonical form is clear as seen from the high merging-phase residual for each against the canonical form (Table II). This is translated as variations in the tetramer packing as revealed from projection density maps for the type I and the three new allomorphs (Fig. 2, first panel). SDS-PAGE on type III and IV crystals, that did not have EDTA in the final buffer, did not indicate enhanced proteolysis when compared to type I crystals that contained EDTA in the final buffer (data not shown). Therefore, the assumption of alternate packing is not due to any

TABLE II
Merging Statistics for the Three New Allomorphs against the Canonical (Type I) Form

	Phase residual ^a	Number of comparisons
Type II	79.5°	226
Type III	59.5°	192
Type IV	77.9°	260

^a Best phase residual for a whole unit cell search. Data included to 6.5 Å resolution. The phase residual between images for the same type ranged from 19.9 to 38.1°.

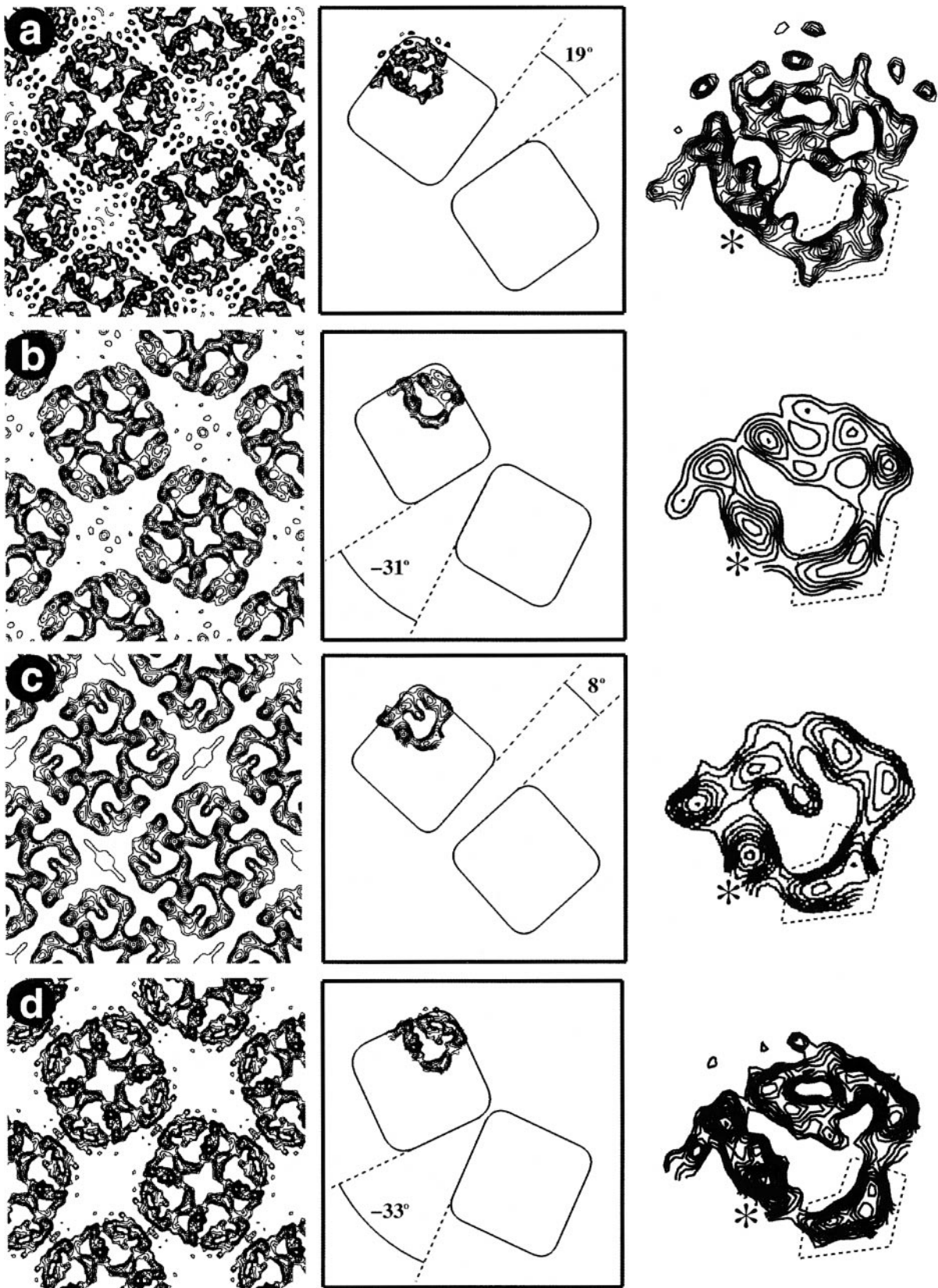


FIG. 2. First panel: Projection density maps showing polymorphism in the packing arrangement of AQP1 tetramers. (a) Map at 3.7 Å resolution of type I form determined in the present study. (b) Map at 6.5 Å resolution determined from type II crystals. (c) Map at 6.5 Å resolution determined from type III crystals. (d) Map at 4 Å resolution determined from type IV crystals. Second panel: The variation in the packing arrangement. The angles between square-shaped schematic representations of a pair of adjacent tetramers in the various allomorphs quantify the packing alteration. The squares define areas that just enclose the strongest peaks of the corresponding projected

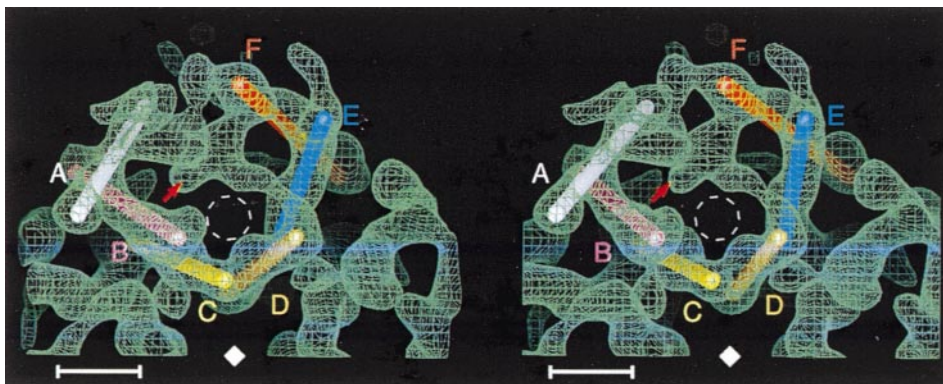


FIG. 3. Stereo pair of 3-D density map of ice-embedded AQP1 at 7 Å resolution (Cheng *et al.*, 1997), viewed approximately perpendicular to the bilayer, showing one monomer and portions of adjacent monomers within a tetramer. The rods trace the approximate paths of the centers of the six tilted α -helices (A to F) that form a barrel surrounding a vestibular region (dashed circle). The arrow indicates the density attributed to the two NPA box regions. Reprinted by permission from *Nature* (Cheng *et al.*, 1997), copyright 1997, Macmillan Magazines, Ltd.

proteolytic cleavage such as that of the protease-sensitive long C-terminal tail (Walz *et al.*, 1996).

Based on the analyses of images recorded under the same conditions (high tension and magnification), the overall average deviation in the individual unit cell dimensions for the three forms (average, calculated variation = $\pm 1.0\%$) when compared to the data for type I (calculated variation = $\pm 1.4\%$) was 2.1 ($\pm 2.0\%$) with the largest deviation being 3.6% (type II). Thus, the calculated unit cell dimensions for the three new allomorphs were similar to that for the type I. Examination of the projection maps for the four different allomorphs (Fig. 2) shows that the interaction between the AQP1 monomers at the interface of the adjacent tetramers in the various allomorphs is quite flexible. This flexibility, which appears as variations in the location and the distance between the region of closest contact between the tetramers, allows for the accommodation of different packing arrangements without large alteration in the cell dimensions. The small differences in the unit cell dimensions for the three allomorphs in comparison to type I may be caused by the LPR in the crystals but not sufficient to account for the difference in the LPR used in reconstitution, for instance, in the case of type II crystals.

The projection density maps in Fig. 2 serve to illustrate and quantify the observed polymorphism. In order to assess the degree of alteration in the packing arrangement of the tetramers, the identifica-

tion of a homologous monomer (tetramer) in the various allomorphs was carried as follows. Since, the same lipid (DOPC) was used throughout and buffer content changed marginally between different crystallization conditions, we expect that the overall 3-D structure of the monomer, its disposition in the bilayer, and the strong intermonomer interaction within a tetramer (Li *et al.*, 1997; Walz *et al.*, 1997; Cheng *et al.*, 1997) are similar in the four allomorphs. This means that the location of the peaks in the projected density of a monomer produced by the tilted helices (Fig. 3) should remain unchanged, or at least similar. In the third panel of Fig. 2, the density map of a monomer excised from tetramer 1 (Fig. 2, second panel) for each of the four allomorphs is provided in order to draw attention to the homologous locations of common features in the monomer densities. For this purpose, the excised densities were approximately aligned by appropriate rotation around the 4-fold axis. Even though, moderate mirror symmetry in the monomer density is apparent around an in-plane axis passing through the center of the tetramer (consistent with previous observation from the 3-D map determined by others and us (Cheng *et al.*, 1997; Li *et al.*, 1997)), features that mark the asymmetry in the density are clearly apparent. In the orientation presented, there is a dense, approximately circular peak on the lower left (marked by an asterisk) which is well separated from other major peaks at a medium resolution (8–6 Å). This peak is known to be generated by the overlap of helix B and C as delineated in the 3-D density map (Fig. 3;

densities (first panel) at the lipid-facing periphery of the tetramers. The orientation of the tetramers in the type I was chosen to designate a positive packing angle (19°). Third panel: The projected density for a monomer in the various allomorphs excised from the tetramer density. In order to help elucidate important, common features of the monomer density, the excised densities were approximately aligned by appropriate rotation around the 4-fold axis (8.5° for type I, -15° for type II, 4° for type III, and -16.5° for type IV). The density peak indicated by a single asterisk and that circumscribed by dotted line identify features that help designate the homologous monomer (and tetramer) in the projected density map shown in the first panel (see text for detail).

Cheng *et al.*, 1997). The density peak at the lower right corner of the monomer (circumscribed by dotted line) is elongated and curved and is due to the overlap of densities for helices C and D, and D and E (Fig. 3). The presence of these distinct, asymmetric features conveys a hand to the projected monomer density and helps distinguish between the density for adjacent tetramers positioned across the diagonal 2-fold axis. Based on the criteria mentioned above and upon close examination of the two possibilities, tetramers identified in Fig. 2 (second panel) were chosen as homologs in the four allomorphs. The relative variation of tetramer disposition in the various allomorphs is given as the change in the angle between adjacent tetramers which varies from $\sim 19^\circ$ for type I to $\sim -33^\circ$ for type IV.

Polymorphism in the packing of a given membrane protein in different types of 2-D crystals has been observed in many cases. Examples are bacteriorhodopsin, rhodopsin, OmpF porin, and microsomal glutathione transferase. Bacteriorhodopsin naturally forms trigonal p3 lattices (Henderson and Unwin, 1975) but orthorhombic crystals can be obtained by reconstitution of purified protein (Michel *et al.*, 1980; Miercke *et al.*, 1991). Depending on the source of protein, purification scheme and the lipid reconstitution protocol, rhodopsin displays different orthorhombic crystal forms (Krebs *et al.*, 1998). OmpF porin shows a variety of crystal forms produced by varying the LPR, by the nature of the lipid, and by phospholipase treatment (Sass *et al.*, 1989; Walian and Jap, 1990; Hoenger *et al.*, 1990; Engel *et al.*, 1992). Minimal changes in the LPR in the case of glutathione transferase engendered marked alterations in the two-sided plane group from p6 to p2₁2₁2 with attendant alteration in the crystal packing (Schmidt-Krey *et al.*, 1999). In all the examples mentioned above, the different packing schemes for a particular membrane protein occur in crystals with different plane group symmetries and consistent with the different symmetry elements in each crystal form. However, as far as we know, our results demonstrate the first example where crystal forms with the same two-sided plane group have been shown to harbor distinct packing arrangements.

The new allomorphs that were generated by (a) the given value of LPR in the crystallization cocktail and (b) the ambient amount of divalent (Mg^{2+}) cation represent different minimum energy states of packing of the tetramer in the lipid milieu. As mentioned above, the role of LPR in controlling the observed crystal packing in other 2-D crystals has been demonstrated. Since types III and IV crystals were generated from type I, the LPR (1:3) is unchanged in these forms. On the other hand, type II crystals are an example of the effect of varying the LPR, which was 1:4. However, as noted above, the lipid content in

type II crystals is similar to that in the other three forms. It appears, therefore, that the relatively reduced amount of lipid present during crystallogenesis of type II leads to alternate favored interactions between the tetramers without producing more dense packing.

Since three of the four allomorphs (type I, III, IV) are distinguished by the level of divalent cations (e.g., Mg^{2+}) in the suspension containing crystals, the strong influence of the cations in modulating crystal packing is apparent. The observation of these multiple forms through treatment of the 2-D crystals also attests to the flexibility of the bilayer membrane. The appearance of the type III form (EDTA free) first indicated to us this possible effect of the divalent cation, which led to experiments that resulted in the generation of type IV crystals. Presumably, the type III form which is generated in the presence of a background level of divalent cation (contaminants in the buffer and leached from the glass dialysis chamber) in EDTA-free buffer represents an intermediate state between type I (with EDTA) and type IV (without EDTA, Mg^{2+} added) forms. In parallel with the altered packing, the images recorded from the type IV crystals consistently showed, among the four allomorphs, the strongest signal at the highest resolution due to the presence of the large coherent areas (Fig. 4). Typical areas of coherent domains in such crystals were $>0.43 \mu\text{m}^2$ (Fig. 4a) compared to $\sim 0.20 \mu\text{m}^2$ for the other forms. A high-resolution computed Fourier transform for a typical image of a type IV crystal is provided in Fig. 4b. In this context, our observations should be contrasted with the results of Walz *et al.* (1994) who observed that addition of divalent cations such as Mg^{2+} or Ca^{2+} (10 to 100 mM) to the reconstitution buffer prevented the formation of vesicles but promoted the growth of mosaic, stacked sheet-like structures whose borders were decorated with aggregated protein. Such sheets apparently were less well ordered compared to the crystals on vesicles. The influence of divalent cation on the surface lattice has been noted before (Wakatsuki *et al.*, 1994) in purple *H. salinarum* membranes containing crystalline patches of bacteriorhodopsin. In this case, upon cation depletion (blue membrane), a distinct lattice structure slightly different from the native form appeared that showed order-disorder transition during dehydration.

The effect of the divalent cation that we observed could be mediated through interaction with phospholipid headgroups, protein side chains, or both. Deuterium NMR studies (Zidovetzki *et al.*, 1989; Roux and Bloom, 1990) have shown that divalent cations such as Mg^{2+} interact more strongly with the phosphatidylcholine headgroup in synthetic lipid bilayers than

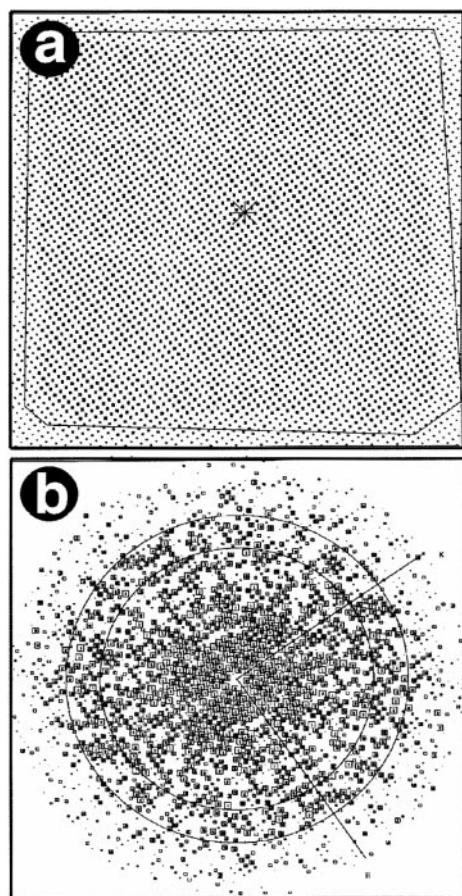


FIG. 4. Highly ordered crystals (type IV) obtained after addition of Mg^{2+} to type I crystals. (a) Very large coherent domain (polygon) in the crystal is indicated by uniformly strong cross-correlation peaks (≥ 0.5 times the maximum peak) when a small reference area of an image not yet corrected for lattice distortions is compared to the rest of the image. (b) Fourier transform of the same image area after corrections for lattice distortion. The size of the squares represents the IQ value (Henderson *et al.*, 1986) of the corresponding reflection. The largest squares represent reflections with IQ equal to 1. The edge of the box is at 3 Å resolution and the circular rings are drawn at 5 and 4 Å resolution.

monovalent cations and can induce conformational change of the headgroup (Roux and Bloom, 1990). In the case of bacteriorhodopsin, the functional role played by divalent cations in the conversion of the blue (inactive) to the purple (active) form of the membrane has been actively studied and has been recently explained (Varo *et al.*, 1999) based on elevation of surface pH produced by nonspecific binding to the surface of the membrane (possibly to the anionic lipid headgroups). For AQP1, there is no published evidence of specific binding of divalent cations except for the special case of inhibitory binding of Hg^{2+} to the extracellular Cys189 (Preston *et al.*, 1993). In the AQP1 polypeptide sequence, however, there are pockets of negatively charged regions in the interhelix loops as well as in the charged C-terminal tail. These

may serve as potential binding sites. In addition, such sites could also exist on the sizable, solvent-accessible, possibly polar surfaces lining the channel on both the cytoplasmic and the extracellular faces that is enclosed by the α -helix barrel (Ren *et al.*, submitted). It is reasonable to argue that some or all of these types of interactions must be at play to produce the observed variations in the packing arrangement. It is interesting to note that among the four forms, the tetramer packing motifs in type II and IV crystals are very similar (packing angles -31 and -33°) (Fig. 2). This suggests that this is a preferred packing scheme which can be accessed either during the process of crystallization starting with protein-lipid-detergent complex or in the protein-reconstituted lipid bilayer.

The averaged discrepancy between the phases for each of the new allomorphs with those for the canonical form is not prohibitively large (Table II). Therefore, the occasional observation of more than one packing allomorph in a AQP1 crystal preparation presents a challenge in the effort to determine the high-resolution structure since images corresponding to the commonly observed type I form must be carefully selected.

CONCLUSION

The main results emanating from this work are summarized below.

1. The packing of AQP1 tetramer in 2-D crystals can show polymorphism.
2. The various packing allomorphs display the same two-sided plane group and similar unit cell dimensions. This has not been observed before in 2-D crystals of any other membrane protein.
3. Variation in the LPR used in the crystallization mixture lead to an altered packing motif of the tetramers.
4. Divalent cation (Mg^{2+}) strongly modulates the packing of AQP1 tetramers in the lipid bilayer. The rotation of the AQP1 tetramers in this case attests to the intrinsic fluidity of the lipid bilayer membrane.

We gratefully acknowledge Dr. B. Jap, Dr. T. Walz, and Dr. A. Engel for contributions to Figs. 1a and 1b. The research was supported by a grant from the National Institutes of Health, a Grant-in-Aid from the American Heart Association, a special fellowship from the Cystic Fibrosis Research Foundation to A. K. M. and a postdoctoral fellowship from the American Heart Association Western affiliate to G. R.

REFERENCES

- Agre, P., Brown, D., and Nielsen, S. (1995) Aquaporin water channels: Unanswered questions and unresolved controversies, *Curr. Opin. Cell Biol.* **7**, 472–483.
- Baldwin, J., and Henderson, R. (1984) Measurement and evaluation of electron diffraction patterns from two-dimensional crystals, *Ultramicroscopy* **14**, 319–336.

- Cheng, A., van Hoek, A. N., Yeager, M., Verkman, A. S., and Mitra, A. K. (1997) Three-dimensional organization of a human water channel, *Nature* **387**, 627–630.
- Dubochet, J., Adrian, M., Chang, J. J., Homo, J. C., Lepault, J., McDowell, A. W., and Schultz, P. (1988) Cryo-electron microscopy of vitrified specimens, *Q. Rev. Biophys.* **21**, 129–228.
- Engel, A., Hoenger, A., Hefti, A., Henn, C., Ford, R. C., Kistler, J., and Zulauf, M. (1992) Assembly of 2-D membrane protein crystals: Dynamics, crystal order, and fidelity of structure analysis by electron microscopy, *J. Struct. Biol.* **109**, 219–234.
- Gorin, M. B., Yancey, S. B., Cline, J., Revel, J. P., and Horwitz, J. (1984) The major intrinsic protein (MIP) of the bovine lens fiber membrane: Characterization and structure based on cDNA cloning, *Cell* **39**, 49–59.
- Grigorieff, N., Ceska, T. A., Downing, K. H., Baldwin, J. M., and Henderson, R. (1996) Electron-crystallographic refinement of the structure of bacteriorhodopsin, *J. Mol. Biol.* **259**, 393–421.
- Hasler, L., Heymann, J. B., Engel, A., Kistler, J., and Walz, T. (1998) 2D crystallization of membrane proteins: Rationales and examples, *J. Struct. Biol.* **121**, 162–171.
- Henderson, R., Baldwin, J. M., Ceska, T. A., Zemlin, F., Beckmann, E., and Downing, K. H. (1990) Model for the structure of bacteriorhodopsin based on high-resolution electron cryo-microscopy, *J. Mol. Biol.* **213**, 899–929.
- Henderson, R., Baldwin, J. M., Downing, K. H., Lepault, J., and Zemlin, F. (1986) Structure of purple membrane from halobacterium halobium: Recording, measurement and evaluation of electron micrographs at 3.5Å resolution, *Ultramicroscopy* **19**, 147–178.
- Henderson, R., and Unwin, P. N. (1975) Three-dimensional model of purple membrane obtained by electron microscopy, *Nature* **257**, 28–32.
- Heymann, J. B., Agre, P., and Engel, A. (1998) Progress on structure and function of aquaporin 1, *J. Struct. Biol.* **121**, 191–206.
- Hoenger, A., Gross, H., Aebi, U., and Engel, A. (1990) Localization of the lipopolysaccharides in metal-shadowed reconstituted lipid-porin membranes, *J. Struct. Biol.* **103**, 185–195.
- Jap, B. K., and Li, H. (1995) Structure of the osmo-regulated H₂O-channel, AQP-CHIP, in projection at 3.5 Å resolution, *J. Mol. Biol.* **251**, 413–420.
- Kimura, Y., Vassilyev, D. G., Miyazawa, A., Kidera, A., Matsushima, M., Mitsuoka, K., Murata, K., Hirai, T., and Fujiyoshi, Y. (1997) Surface of bacteriorhodopsin revealed by high-resolution electron crystallography, *Nature* **389**, 206–211.
- Krebs, A., Villa, C., Edwards, P. C., and Schertler, G. F. (1998) Characterisation of an improved two-dimensional p22121 crystal from bovine rhodopsin, *J. Mol. Biol.* **282**, 991–1003.
- Kühlbrandt, W., Wang, D. N., and Fujiyoshi, Y. (1994) Atomic model of plant light-harvesting complex by electron crystallography, *Nature* **367**, 614–621.
- Li, H., Lee, S., and Jap, B. K. (1997) Molecular design of aquaporin-1 water channel as revealed by electron crystallography [letter] [see comments], *Nature Struct. Biol.* **4**, 263–265.
- Michel, H., Oesterhelt, D., and Henderson, R. (1980) Orthorhombic two-dimensional crystal form of purple membrane, *Proc. Natl. Acad. Sci. USA* **77**, 338–342.
- Miercke, L. J., Betlach, M. C., Mitra, A. K., Shand, R. F., Fong, S. K., and Stroud, R. M. (1991) Wild-type and mutant bacteriorhodopsins D85N, D96N, and R82Q: Purification to homogeneity, pH dependence of pumping, and electron diffraction, *Biochemistry* **30**, 3088–3098.
- Mitra, A. K., Yeager, M., van Hoek, A. N., Wiener, M. C., and Verkman, A. S. (1994) Projection structure of the CHIP28 water channel in lipid bilayer membranes at 12-Å resolution, *Biochemistry* **33**, 1273S–12740.
- Mitra, A. K., van Hoek, A. N., Wiener, M. C., Verkman, A. S., and Yeager, M. (1995) The CHIP28 water channel visualized in ice by electron crystallography [letter], *Nature Struct. Biol.* **2**, 726–729.
- Nakhoul, N. L., Davis, B. A., Romero, M. F., and Boron, W. F. (1998) Effect of expressing the water channel aquaporin-1 on the CO₂ permeability of *Xenopus* oocytes [see comments], *Am. J. Physiol.* **274**, C543–C548.
- Prasad, G. V., Coury, L. A., Finn, F., and Zeidel, M. L. (1998) Reconstituted aquaporin 1 water channels transport CO₂ across membranes, *J. Biol. Chem.* **273**, 33123–33126.
- Preston, G. M., Jung, J. S., Guggino, W. B., and Agre, P. (1993) The mercury-sensitive residue at cysteine 189 in the CHIP28 water channel, *J. Biol. Chem.* **268**, 17–20.
- Ren, G., Cheng, A., Melnyk, P., and Mitra, A. K. Three-dimensional fold of the human AQP1 water channel determined by electron crystallography of 2-dimensional crystals embedded in ice, submitted for publication.
- Roux, M., and Bloom, M. (1990) Ca²⁺, Mg²⁺, Li⁺, Na⁺, and K⁺ distributions in the headgroup region of binary membranes of phosphatidylcholine and phosphatidylserine as seen by deuterium-NMR, *Biochemistry* **29**, 7077–7089.
- Sass, H. J., Buldt, G., Beckmann, E., Zemlin, F., van Heel, M., Zeitler, E., Rosenbusch, J. P., Dorset, D. L., and Massalski, A. (1989) Densely packed beta-structure at the protein-lipid interface of porin is revealed by high-resolution cryo-electron microscopy, *J. Mol. Biol.* **209**, 171–175.
- Schertler, G. F., Villa, C., and Henderson, R. (1993) Projection structure of rhodopsin, *Nature* **362**, 770–772.
- Schmidt-Krey, I., Murata, K., Hirai, T., Mitsuoka, K., Cheng, Y., Morgenstern, R., Fujiyoshi, Y., and Hebert, H. (1999) The projection structure of the membrane protein microsomal glutathione transferase at 3Å resolution as determined from two-dimensional hexagonal crystals, *J. Mol. Biol.* **30**, 243–253.
- van Hoek, A. N., Wiener, M. C., Verbavatz, J. M., Brown, D., Lipniunas, P. H., Townsend, R. R., and Verkman, A. S. (1995) Purification and structure-function analysis of native, PNGase F-treated, and endo-β-galactosidase-treated CHIP28 water channels, *Biochemistry* **34**, 2212–2219.
- Varo, G., Brown, L. S., Needleman, R., and Lanyi, J. K. (1999) Binding of calcium ions to bacteriorhodopsin, *Biophys. J.* **76**, 3219–3226.
- Verkman, A. S., van Hoek, A. N., Ma, T., Frigeri, A., Skach, W. R., Mitra, A., Tamarappoo, B. K., and Farinas, J. (1996) Water transport across mammalian cell membranes, *Am. J. Physiol.* **270**, C12–C30.
- Wakatsuki, S., Kimura, Y., Stoeckenius, W., Gillis, N., Eliezer, D., Hodgson, K. O., and Doniach, S. (1994) Blue form of bacteriorhodopsin and its order-disorder transition during dehydration, *Biochim. Biophys. Acta* **28**, 160–166.
- Walian, P. J., and Jap, B. K. (1990) Three-dimensional electron diffraction of PhoE porin to 2.8 Å resolution, *J. Mol. Biol.* **215**, 429–438.
- Walz, T., Hirai, T., Murata, K., Heymann, J. B., Mitsuoka, K., Fujiyoshi, Y., Smith, B. L., Agre, P., and Engel, A. (1997) The three-dimensional structure of aquaporin-1, *Nature* **387**, 624–627.
- Walz, T., Tittmann, P., Fuchs, K. H., Muller, D. J., Smith, B. L., Agre, P., Gross, H., and Engel, A. (1996) Surface topographies at subnanometer-resolution reveal asymmetry and sidedness of aquaporin-1, *J. Mol. Biol.* **264**, 907–918.
- Walz, T., Typke, D., Smith, B. L., Agre, P., and Engel, A. (1995)

- Projection map of aquaporin-1 determined by electron crystallography [letter], *Nature Struct. Biol.* **2**, 730–732.
- Walz, T., Smith, B. L., Zeidel, M. L., Engel, A., and Agre, P. (1994) Biologically active two-dimensional crystals of aquaporin CHIP. *J. Biol. Chem.* **269**, 1583–1586.
- Zeidel, M. L., Nielsen, S., Smith, B. L., Ambudkar, S. V., Maunsbach, A. B., and Agre, P. (1994) Ultrastructure, pharmacologic inhibition, and transport selectivity of aquaporin channel-forming integral protein in proteoliposomes, *Biochemistry* **33**, 1606–1615.
- Zidovetzki, R., Atiya, A. W., and De Boeck, H. (1989) Effect of divalent cations on the structure of dipalmitoylphosphatidylcholine and phosphatidylcholine/phosphatidylglycerol bilayers: an ²H-NMR study, *Membr. Biochem.* **8**, 177–186.